Surface Vibration Measurement and Analysis for UAM/UAS Electric Motor Noise

Jordan D. Cluts[1], Dennis L. Huff[2], Brenda S. Henderson[2], and Charles Ruggeri[3]
NASA Glenn Research Center, Cleveland, Ohio, 44135, USA

Urban Air Mobility vehicles are an emerging class of vertical lift vehicles using electric motors to drive multiple rotors for lift. The outrunner electric motors that are commonly used, may be capable of generating noise that could contribute to the vehicle's overall noise profile and could generate cabin noise. Understanding and predicting the noise requires more knowledge of the rotor vibrations and eventually a model to predict the frequencies of those vibrations. This work presents a measurement of the rotor vibrations of two different small-scale motors. Two techniques to measure the surface vibration were used. The displacement spectra are compared with acoustic measurements. A finite element analysis model is used to predict the rotor resonance frequencies. The predicted frequencies are in fair agreement with the experimentally observed vibration frequencies, but requires further work to understand discrepancies.

I. Introduction

Urban Air Mobility (UAM) and Unmanned Aerial Systems (UAS) represent an emerging field of electrified and hybrid-electric aircraft to carry cargo, passengers, and other payloads on short range flights. These vehicles typically have a multi-rotor vertical takeoff capability allowing for "vertiports" serving a small surrounding region. The impact of noise generated by these vehicles on the communities they serve could be a factor in the acceptance and success of this emerging market. As a result, the ability to understand and predict the noise generated is important for further development. A recent white paper on UAM noise has identified the challenges and goals for research [1]. The current work is aimed at understanding and predicting electric motor noise for these vehicles.

All-electric vertical takeoff vehicles, designated eVTOL (electric vertical takeoff and landing), will have noise originating from the rotors and surrounding surfaces. The noise consists of propeller tones and broadband noise resulting from rotor self-noise and interaction sources. Another potential noise source is the electric motors used for propulsion [2, 3]. Noise generated by the electric motor may contribute to community impacts during aircraft flyovers and could contribute to vehicle cabin noise via motor structure interactions. The relative importance of this source on the overall sound level is unknown due to the lack of acoustic data for large scale eVTOL vehicles.

Since many of these vehicles are emerging conceptually, the motor architecture is still evolving. Conventional motors have the rotor located inside the stator containing the magnetic poles. Many of the UAM applications use "outrunner" motors where the rotor is exposed and becomes a radiating surface for noise [4, 5]. The noise generated by the rotor structural vibration varies with motor speed and is excited by the magnetic field. This paper focuses on the rotor structural vibrations in an outrunner motor during operation.

A system-level analysis tool to predict noise of UAM vehicles will require a structural analysis of the vibration modes of the rotor. Many source modules for similar prediction codes use semi-empirical methods due to requirements for computational efficiency [6]. Since electric motors have a variety of geometric features that impact the structural vibration characteristics, the development of a semi-empirical method that can reliably predict important resonant frequencies contributing to noise is a challenge. This task is further complicated by the impact of variable RPM present

[1] Research Aerospace Engineer, Acoustics Branch, AIAA Member.
[2] Research Aerospace Engineer, Acoustics Branch, AIAA Associate Fellow.
[3] Structural Dynamics Engineer, Structural Dynamics Branch.

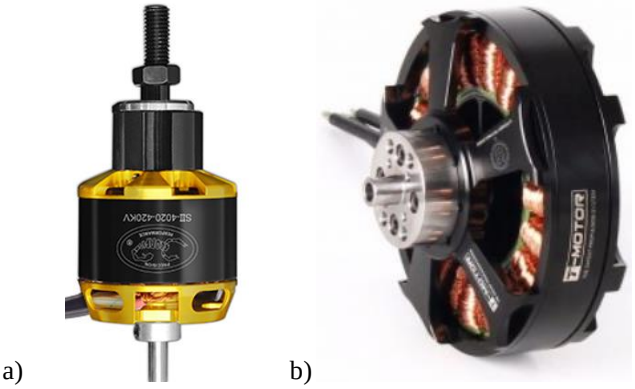
in these vehicles. An RPM change will alter the forcing provided by the electro-magnetic field and can also cause changes in the rotor resonance frequencies [7].

Finite element methods can be used to parameterize the problem with the hope of deriving a simplified model of the rotor vibration and resonance. As a first step, validation data is needed for comparison of the structural vibration amplitudes with predictions. The focus of this paper is to explore methods for measuring the vibration amplitudes of a rotating surface from a motor and compare the results with finite element predictions.

This paper details the experiment and method to measure the surface vibrations of an outrunner motor in Section II. Time histories of surface displacement obtained via two different methods are compared to one another to show their qualitative similarities in Section III. In Section IV, the spectra of the surface displacement are related to far-field acoustic spectra. Peaks in the surface displacement spectra align with tones in the acoustic spectra, indicating that the surface vibrations are related to the observed acoustic tones. Finally, Section V discusses a finite element model of the rotors. The mode shapes and frequencies the model predicts are compared to the surface displacement spectra in Section VI.

II. Vibration Measurement Experimental Methodology

Two different electric motors were tested. An image of each motor, a Scorpion SII-4020 and a T-Motor U13 are shown in Fig. 1. Both motors are brushless outrunner electric motors. The Scorpion motor has a relatively high aspect ratio (height/diameter) whereas the U13 aspect ratio is much lower.



a) b)

Fig. 1 a) Scorpion SII-4020-420kV Outrunning Electric Motor, b) T-Motor U13 KV100 Outrunning Electric Motor

Two different measurement techniques were used to measure the radial rotor surface displacement. The motors as well as the measurement devices were mounted on an optical table. The two measurement devices are arranged relative to the motor as depicted in Fig. 2. The first measurement device is a Polytec OFV-5000 Laser Vibrometer. The laser vibrometer combines a laser emitter and receiver and extracts surface displacement data by comparing the emitted laser from that received from a reflection from the target surface. The target point in this experiment is the rotor surface which has a horizontal white stripe (not shown in Fig. 1) painted on in order to increase the surface reflectivity. Because the laser vibrometer measures displacement parallel to the laser beam, it is crucial to align the laser vibrometer perpendicular to the rotor surface. If the beam is not perpendicular to the surface, a component of the rotational velocity of the rotor is parallel to the beam. This surface velocity is then measured by the laser vibrometer and easily overwhelms the vibration of the rotor surface.

The second technique is a 2D photogrammetry method that uses a telecentric lens paired with a Photron SA-Z high-speed camera. The camera is aligned tangential to the motor bell housing as depicted in Fig. 2 such that a radial change in the bell housing equates to an in-plane displacement in the cameras field of view. Using an Opto Engineering® telecentric lens paired with a collimated light source eliminates perspective errors in the image and also provides magnification. The lens has a diameter of 90 mm and provides a magnification of 0.56. Images where taken at 100k frames per second with a resolution of 896 pixels by 104 pixels with exposure times in the 2-4 µs range. Fig. 4 shows the U13 motor and the rotor area imaged as well as a typical image captured by the high-speed camera rotated 90 degrees to the experimental setup seen in Fig. 2. The scale for the FOV was measured using a glass scale with 2 mm graduations located at the focal plane of the lens.

Images were analyzed using Image Systems© TEMA motion analysis software using its subpixel edge detection tool. The detection area was set to an area of 5-by-5 pixels and its movement constrained in the vertical direction such that only the horizontal motion (radial in respect to the motor) was captured (see Fig. 2). The magnitude of the surface vibration is smaller than the pixel pitch but the subpixel detection routine can still extract the surface displacement. Two measurements were made in each test, one located about 1/4 of the length of the bell housing and another located about 3/4 of the vertical length. To account for camera and motor mount vibrations the base of the motor was tracked and any global movement was subtracted from the bell housing measurements. Displacement data was filtered using a low pass channel frequency class 7000 filter which has a cutoff frequency around 11.5kHz.

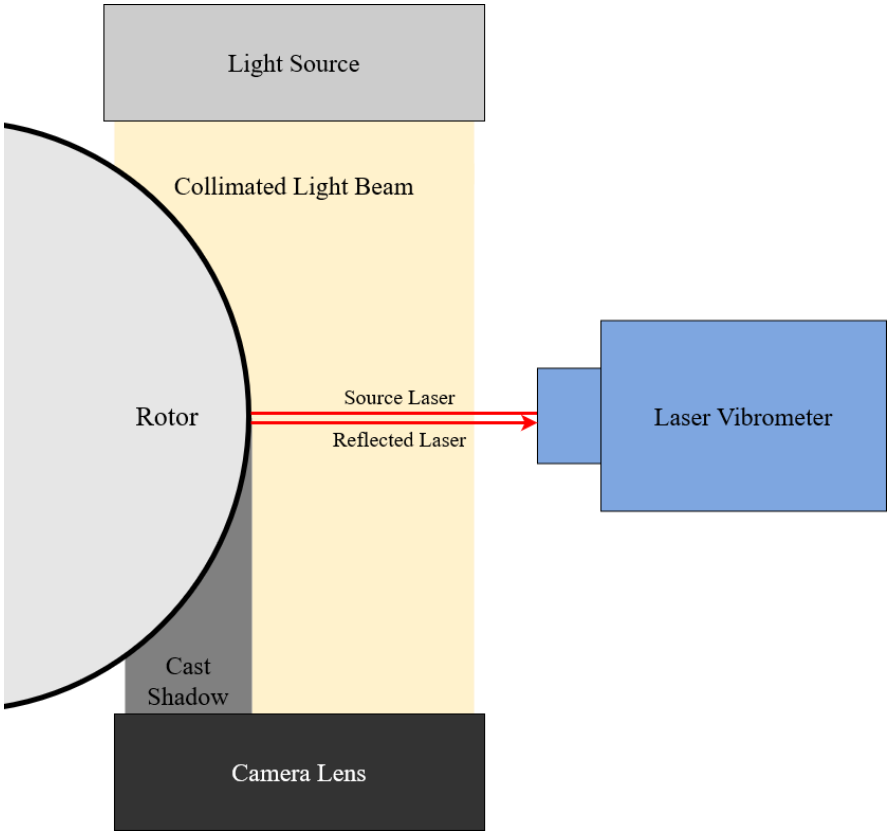


Fig. 2 Diagram of photogrammetry and laser vibrometer arrangement

By arranging the two devices perpendicular to one another as depicted in Fig. 2 they simultaneously measure the displacement of the rotor's surface at the same azimuthal location. The photographic method, however, observes the entire vertical extent of the rotor allowing the surface displacement at any point to be extracted via an edge detection tool. Two points have been extracted from the photogrammetry data as depicted in Fig. 3 referred to as Photogrammetry Point 1 and 2, respectively.

The two measurements from each device were taken simultaneously but without synchronization. The sampling rate was also different for the two measurements but the data postprocessing of each was similar. A 500 Hz high-pass filter was applied to remove motor mount vibrations as well as once-per-revolution effects such as rotor surface imperfections.

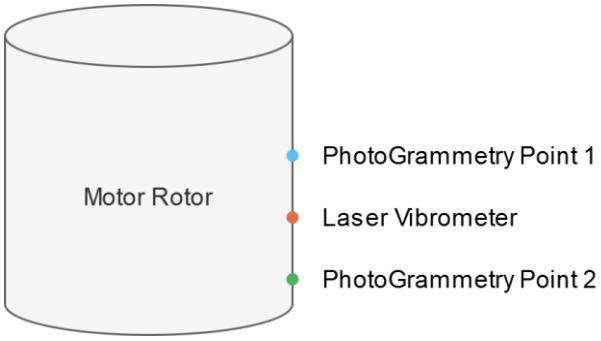
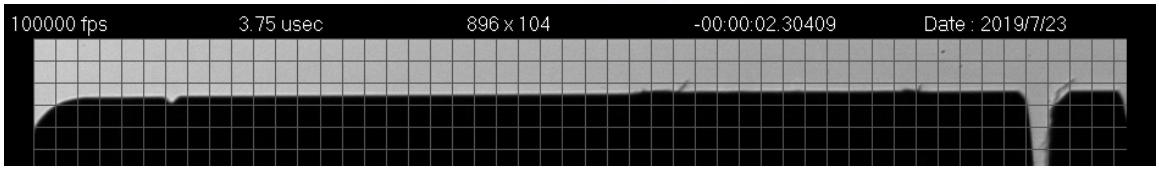


Fig. 3 Relative Position of Photogrammetry Points extracted and Laser Vibrometer Measurement Point. Not to Scale



a)



b)

Fig. 4 a) U13 motor with area of camera focus, b) U13 rotor surface as observed by collimated light beam

III. Detection of Rotor Surface Vibrations

Comparisons between the time histories of the surface displacement measured by the two techniques on the Scorpion motor are shown in Fig. 5. The two time histories represent a 10 millisecond sample of data taken while the motor operated at 6850 RPM. At this rpm, 10 milliseconds represents 411° of rotation of the rotor. Note that while both samples are 10 milliseconds in length and were acquired during the same operation of the Scorpion motor, the two systems were not synchronized and so the time windows shown do not overlap. Despite this, the two time histories are qualitatively similar. It is clear that both exhibit a periodic displacement with a peak-to-peak amplitude on the order of 2 μm.

A similar set of data for the U13 motor at a rotational rate of 3007 RPM is shown Fig. 6. The displacement time history shows a periodic behavior even more clearly than the Scorpion. The laser vibrometer shows an approximate peak-to-peak amplitude of 5-7 μm. This peak-to-peak value varies in amplitude over the course of the sample. The

photogrammetry data has a peak-to-peak value closer to 3-4 μm, both of these peak-to-peak displacements are larger than observed in the Scorpion motor. While the overall displacement in the U13 is larger than the Scorpion, there is a larger discrepancy observed between the two measurement techniques.

To further compare the displacement results, the power spectra are calculated from the displacement data. The power spectra for both photogrammetry points and the laser vibrometer are shown in Fig. 7. This data is for the U13 motor operating at 3007 RPM, a large peak in the power spectra is observed at 1255 Hz in all three measurements. Each of the three measurement points is at a different location on the rotor surface. The presence of the same frequency at different measurement locations indicates the movement is of the entire rotor surface. While there is a difference in the magnitude of the peak obtained by the two measurement techniques, the close agreement in frequency is encouraging evidence that a real signal is being measured.

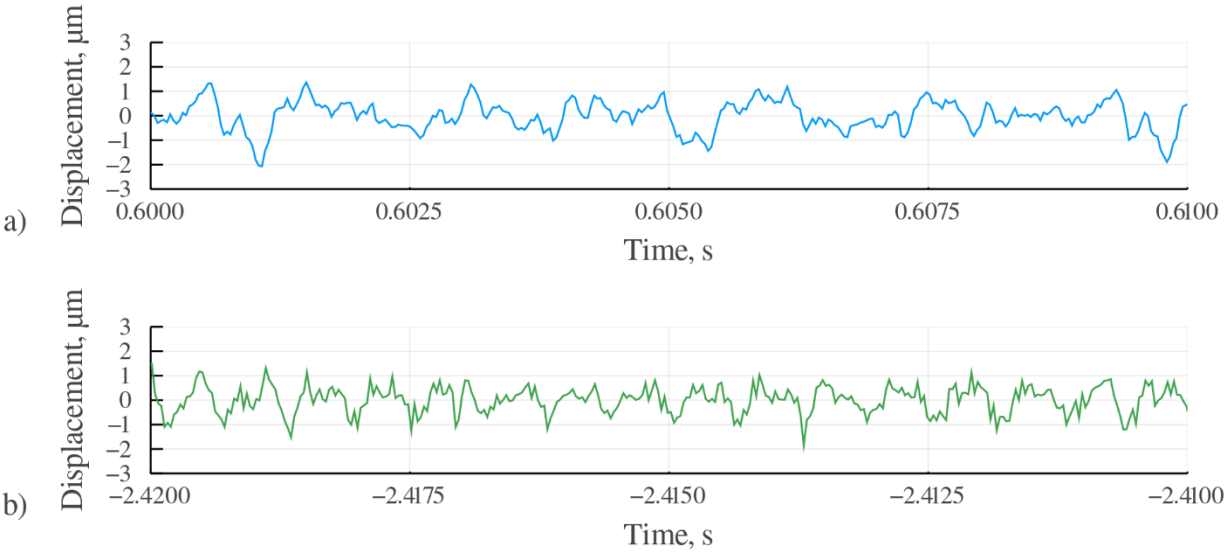


Fig. 5 Scorpion SII-4020 surface displacement at 6850 RPM measured by a) the laser vibrometer and b) photogrammetry

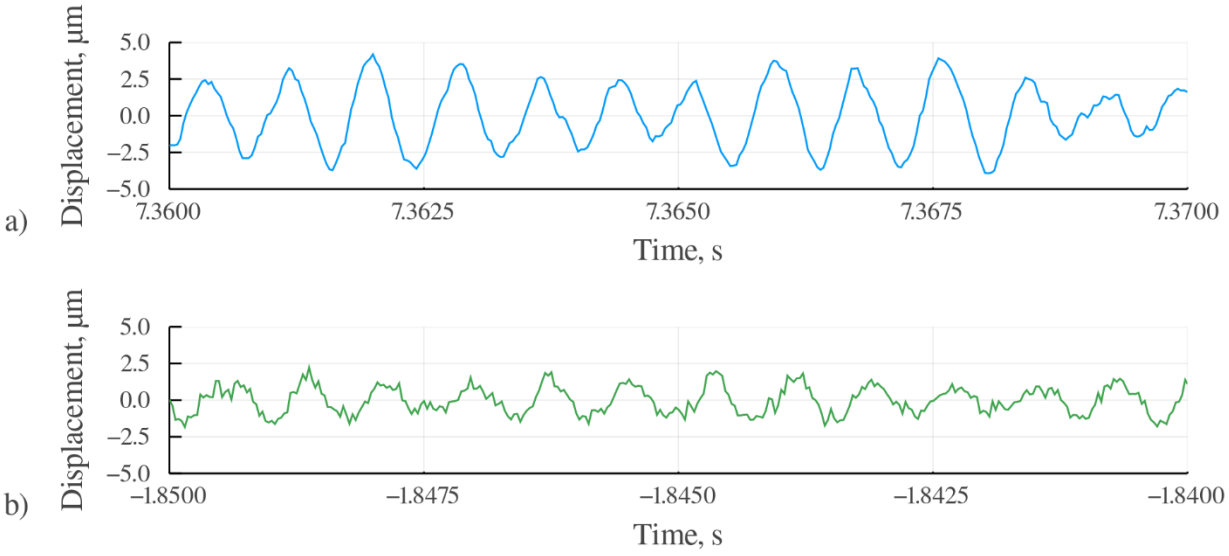


Fig. 6 U13 surface displacement at 3007 RPM measured by a) the laser vibrometer and b) photogrammetry

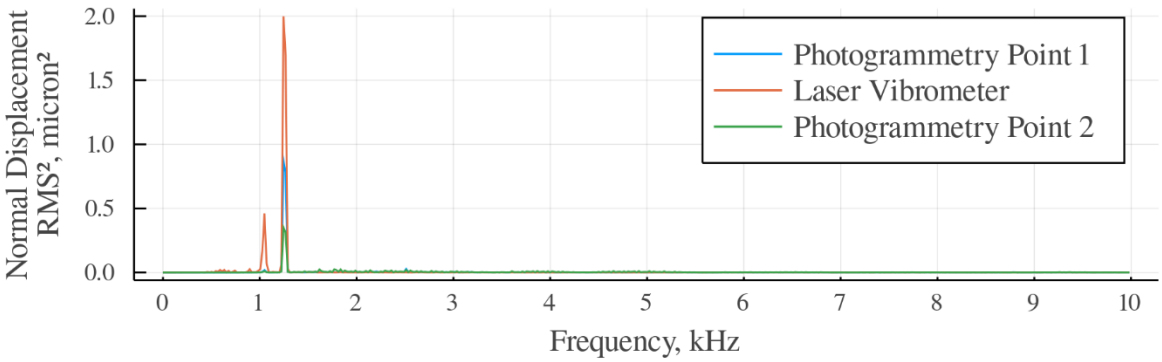


Fig. 7 U13 Power Spectra at 3007 RPM

IV. Comparison with Experimental Results

Far field acoustic measurements were made for the U13 and Scorpion motors in the Acoustic Testing Laboratory. Details of these acoustic measurements can be found in [8, 9]. While the mounting and measurement techniques are the same as those used in the previous studies, the motors used here are different. The arrangement of microphones used in the acoustic measurements are depicted in Fig. 8. The 6 microphones form a 1 m arc perpendicular to the plane of rotation of the motor. Microphone 1 is parallel to the axis of rotation, but aligned with the motor edge, while Microphone 4 is in the plane of the motor, pointed directly at the center of the rotor.

Fig. 9 a) displays acoustic data of the Scorpion motor operating at 6870 RPM. There is an acoustic peak near 3.2 kHz. Another small peak in the spectra is visible near 1.7 khz.

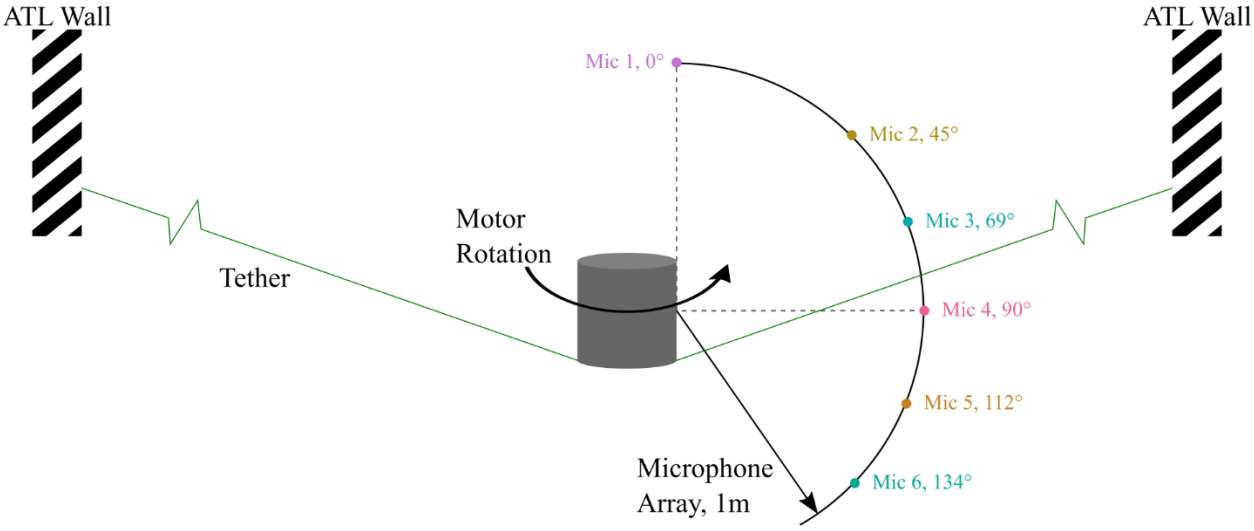


Fig. 8 Acoustic Measurement Microphone Arrangement

Fig. 9 b) shows the Scorpion surface displacement power spectra operating at 6850 RPM. 6850 RPM is similar although not identical to the operating speed represented by the acoustic data in Fig. 9 a). A peak near 3210 Hz is observed in all three measurement locations. This peak appears to correspond to the acoustic tone. The photogrammetry point 2 also measured a peak near 1.7 kHz that matches a peak in the acoustic data. This frequency was not observed in the other displacement measurements points.

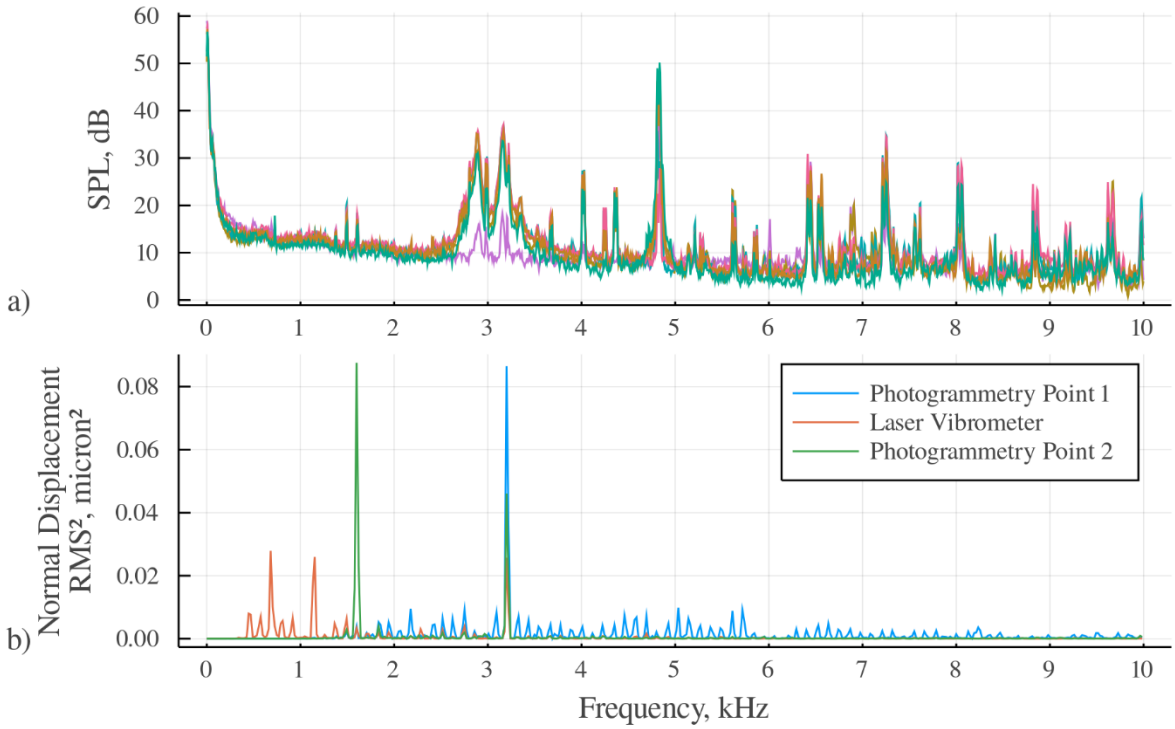


Fig. 9 a) SPL acoustic measurements of a Scorpion motor operating at 6870 RPM as observed at the microphone locations indicated in Fig. 8, b) Scorpion Power Spectra at 6850 RPM

A similar comparison is performed for the U13 motor operating at 2968 RPM. Fig. 10 a) shows the acoustic data from the microphone arc and the power spectra is shown in Fig. 10 b). Both the acoustic sound-pressure level and the power spectra show a peak around 2.8 kHz. In both motors, there is a correlation between measured surface vibrations and acoustic tones generated by the motor.

The acoustic measurements depicted in both Fig. 9 and Fig. 10 also show tones occurring near 8 kHz. The acoustic results are for different motors operating at different speeds so the existence of tones near 8 kHz in both cases is coincidental. However surface displacements were not observed using either measurement technique for frequencies above 5 kHz. It is possible that as these measurements were taken at separate times and with the motors mounted differently that the motor did not resonate at this frequency during the surface displacement measurements. More likely, the displacement measurements are unable to detect these modes. The amplitude of vibrations is approximately 2 μm for the Scorpion and 5 μm for the U13. This displacement amplitude is near the sensitivity limit of both the Laser Vibrometer and the Photogrammetry techniques. It is possible that these higher frequency tones are generated by vibrations with a slightly smaller amplitude that is not well resolved by the direct measurements.

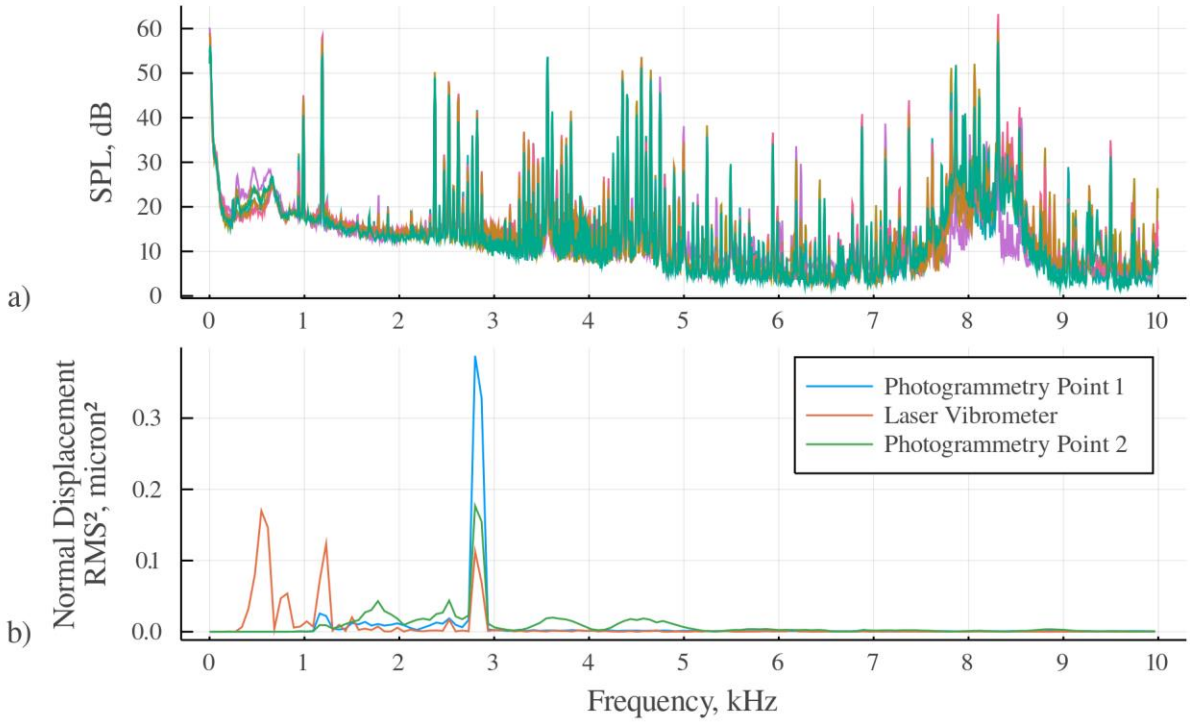


Fig. 10 a) SPL acoustic measurements of the U13 motor operating at 2968 RPM as observed at the microphone locations indicated in Fig. 8, b) U13 Power Spectra at 2968 RPM

V. Rotor Finite Element Simulation

A finite element model of the motors was created. A model of the geometry of each rotor was created in SolidWorks. A rendering of the geometries is shown in Fig. 11. Each geometry was then imported into COMSOL MultiPhysics® for finite element analysis. The default physics based meshing routine was used to generate the meshes.

The finite element model was used to perform an eigenfrequency and mode shape analysis. The simulation used here is relatively simple. Only the rotor was modeled so the effects of the stator mass and magnetic interaction between rotor and stator were not included. The aim of the model is to compare the predicted frequencies and mode shapes with those observed experimentally. An example of one of the predicted mode shapes is depicted in Fig. 12. This mode is the azimuthal mode 2 vibration, predicted by the model to occur at 3939 Hz. The amount of surface displacement is highest at the bottom rotor lip and decreases as one moves towards the spokes.

The COMSOL simulation predicts a number of modes for each motor. In Table 1 and Table 2, the first six predominantly circumferential modes for the Scorpion and U13 motors are listed. The modes are distinguished by their azimuthal mode number (m) and the axial mode number (n). Two frequencies, corresponding to the clockwise and counterclockwise travelling modes of each shape are predicted by the simulation. For each mode shape only the lower frequency of the pair is listed for brevity. A number of more complex modes are also predicted by the simulation. These modes often involve more axial movement of the spokes. Discussion and analysis of these more complex mode shapes will be addressed in future publications.

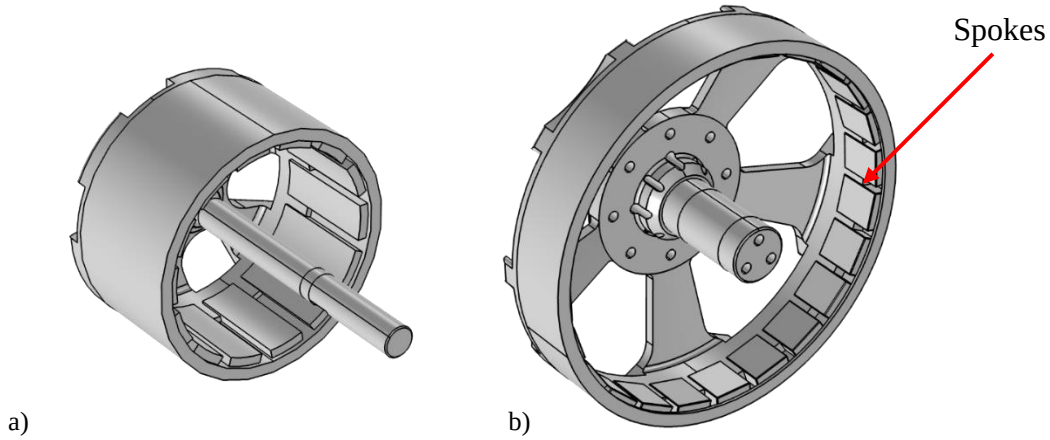


Fig. 11 Simulation geometry of a) the Scorpion Rotor and b) the U13 Rotor

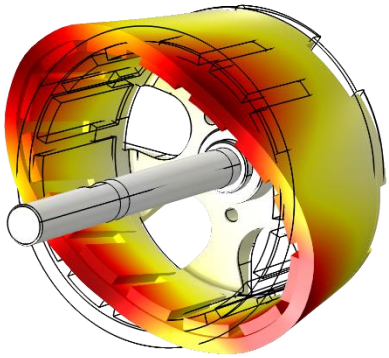


Fig. 12 Scorpion rotor showing simulated azimuthal mode 2 vibration at 3938.6 Hz

Table 1 Scorpion SII-4020 Simulated Mode Shapes and Frequencies

Mode, m,n	Frequency, Hz
1,1	**1114**
2,1	**3939**
3,1	**9409**
4,1	**16594**
3,2	**22731**
5,1	**25010**

Table 2 T-Motor U13 Simulated Mode Shapes and Frequencies

Mode, m,n	Frequency, Hz
1,1	**439**
2,1	**1354**
3,1	**3273**
4,1	**5513**
5,1	**7434**
6,1	**11284**

At any given rotation rate each motor will exhibit some but not all of the modes predicted by the simulation. This is caused by different speeds resonating with some but not all of the mode frequencies. Which subset of the modes are physically exhibited can therefore vary with RPM. The FEA simulation predicts all of the rotor modes as it does not capture these changing resonances. There is however another way the FEA can vary with RPM. Due to centrifugal stiffening it is possible that the frequency of a given mode will vary as the simulated RPM varies [7]. To test the impact this may have, rotation was added to the simulation. Each rotor was then simulated at several representative rotation rates including 0 RPM. Fig. 13 shows the predicted frequencies of several modes for the Scorpion motor at 4 rotational speeds. Only very slight changes in the predicted frequency for each mode occurred with most differences on the order of 1 Hz. A similar result was obtained for the U13 motor. Consequently, we conclude that our model is insensitive to RPM. Due to the insensitivity of the model to RPM the simulation results given in Table 1 and Table 2 as well as plotted in Fig. 14 and Fig. 15 were calculated with a simulated RPM of 0.

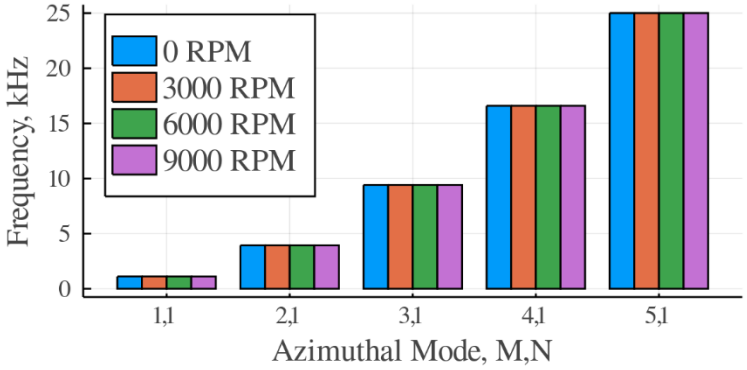


Fig. 13 Scorpion Simulation RPM Sensitivity Study

VI. Experimental and Simulation Comparisons

The FEA predicted mode frequencies can be compared with the surface displacement power spectra. Fig. 14 shows the power spectra for the U13 motor at two speeds. The predicted frequencies are indicated by the purple points. The amplitude for the predictions was chosen arbitrarily for clarity. In Fig. 14 a), for the U13 operating at 2968 RPM, the laser vibrometer has a peak near 1200 Hz. This is near the FEA predicted frequency of 1358 Hz. All 3 surface displacement measurements show a peak around 2.8 kHz which is believed to correspond to predicted mode at 3273 Hz.

Fig. 14 b) plots the same model predicted points with the power spectra of the U13 at 3007 RPM. The peak in the power spectra near 1200 Hz has increased in amplitude and is now detected in all 3 spectra. Conversely, the peak near 2.8 kHz is no longer observed. The change from one observed frequency to another has occurred with only a 1.3% change in RPM.

It has been shown [9] that the electronic speed controllers used to drive small brushless outrunner motors can produce an electro-magnetic-field with rich spectral content. The magnetic field imparts a fluctuating force on the rotor magnets, driving vibrations of the rotor. The rotor of a given electric motor will have several resonant frequencies. Given the many harmonics in the electro-magnetic spectra, at any given motor RPM it is likely that some of the harmonic frequencies will be close to the motor resonance frequencies. When one of the frequencies of the magnetic field aligns with one of the motor resonance frequencies, the motor is at a critical RPM and the motor vibration level is expected to peak for that frequency. At other rotation speeds, none of the electro-magnetic-field frequencies perfectly match a rotor resonance frequency. In this case, the rotor will vibrate at the electro-magnetic-field frequency and have a lower vibration amplitude than at the critical motor speed. The closer the field frequency is to the resonance frequency, the larger the induced vibration. At different motor speeds different rotor resonances will be more closely matched by the electro-magnetic field fluctuations, causing the vibration frequency to vary.

The FEA model predicts the resonant frequencies of the rotor. When the motor is operating at a critical speed the observed vibration should be relatively large and close in frequency to that predicted by the model. At non-critical speeds the vibrations will be smaller and will occur at frequencies near but not identical to those predicted by the model.

It is not known if the U13 motor in Fig. 14 was operating at a critical speed in either instance. At 3007 RPM, due to the larger vibration amplitude and closer agreement with predicted resonant frequency, the motor is likely closer to

a critical frequency than when operated at 2968 RPM. The change in observed vibration frequency and amplitude resulting from a small change in RPM demonstrates the sensitivity of the rotor resonance to RPM.

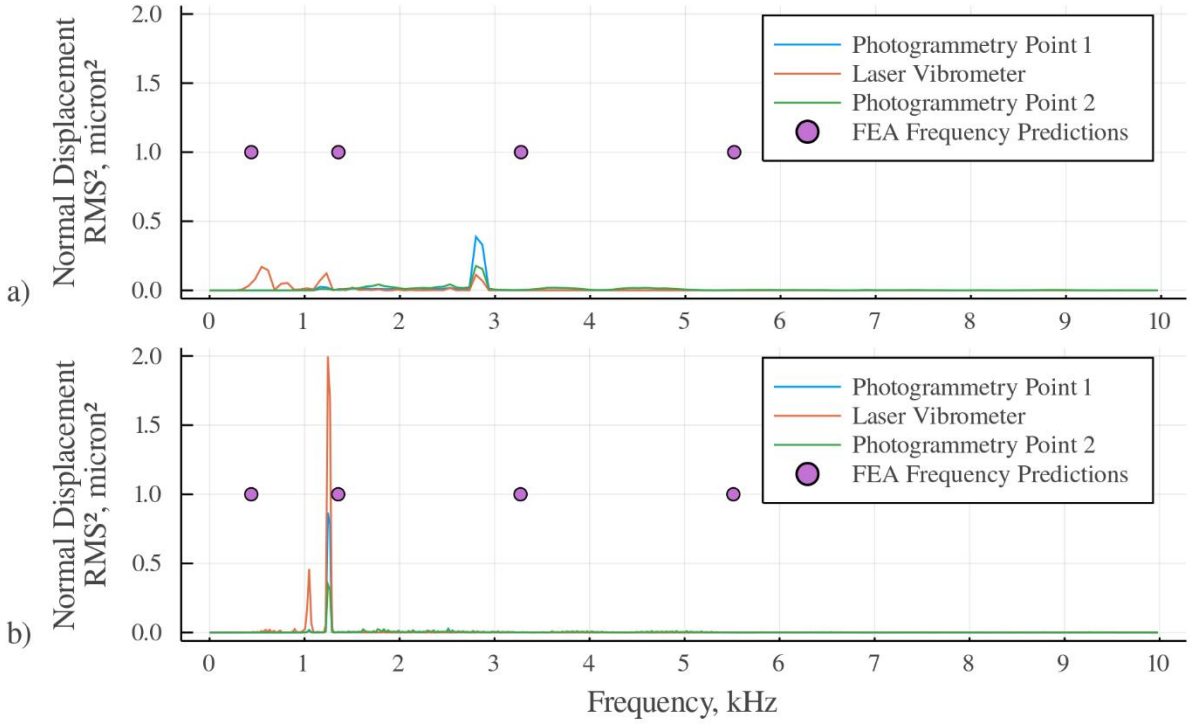


Fig. 14 Comparison of the frequency of modes predicted by FEA compared with displacement power spectra for the U13 motor at a) 2968 RPM and b) 3007 RPM

A similar comparison for the Scorpion motor is made in Fig. 15. Unlike the speeds shown for the U13 which differed only slightly, the two rotation rates presented for the Scorpion motor are quite different, the higher speed being more than twice the lower. Like the U13 power spectra, both Scorpion spectra show different peaks between the two speeds. This is less surprising given the disparate rotation rates, but shows that even at low operating speeds the rotor can resonate and generate a detectable surface vibration.

The FEA modeling predicts two modes below 5 kHz, the first at 1114 Hz and the second at 3939 Hz. While neither correspond perfectly to any observed vibrations, there are multiple peaks at frequencies near those predicted. The critical speeds are again unknown so the peaks may not perfectly match the predictions in frequency. The surface displacement power spectra does have a small peak near 1200 Hz at the higher speed which corresponds more closely to a predicted frequency. This small peak while the motor operates at 6850 RPM as well as the larger peak near 800 Hz at 3055 RPM likely correspond to the Mode 1 vibration predicted by FEA at 1114 Hz.

The results are suggestive that the FEA model is capturing the resonant frequencies of the rotors. Future work to explore the more complex modes predicted by the model, as well as further measurement of electric motor rotor vibrations will aim to improve the predictions.

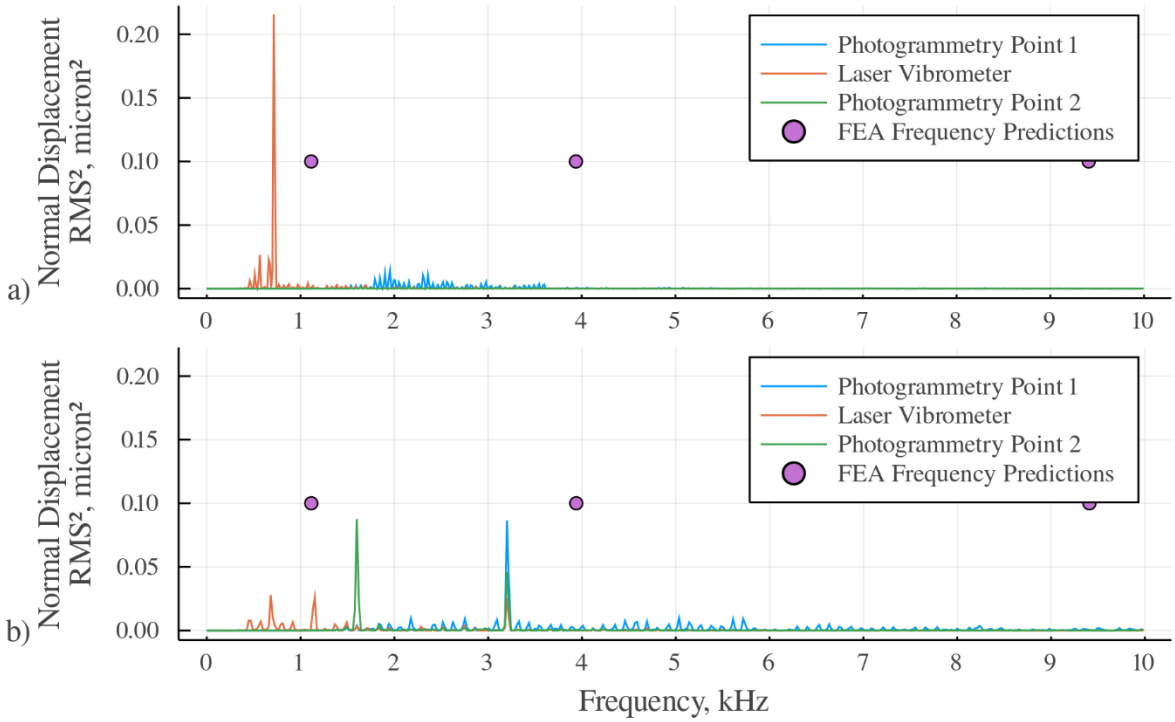


Fig. 15 Comparison of the frequency of modes predicted by FEA compared with displacement power spectra for the Scorpion motor at a) 3055 RPM and b) 6850 RPM

VII. Conclusion

Rotor vibration data were acquired from two brushless DC outrunner motors at multiple operating speeds. Two different techniques, photogrammetry and laser vibrometer were simultaneously used to measure rotor surface vibrations. The data were processed to compare with one another and periodic surface fluctuations on the order of 2-7 μm were detectable in both time histories.

The spectra of the surface displacement data were compared with far-field acoustic measurements, measured acoustic tones are observed to correspond to peaks in the surface displacement spectra for low frequencies. The surface displacement measurements do not show peaks at frequencies above 5 kHz. The correspondence between acoustic tones and rotor surface vibrations is evidence that these tones are in fact generated by the vibration of the rotor. Further investigation will be needed to understand why vibrations were not detected at higher frequencies, whether due to their absence caused by differences in experimental setup, or due to being beyond the capability of the experimental tools.

An FEA model of the electric motor rotor was built to predict the resonance frequencies of the rotor. These predicted frequencies were also compared with the surface displacement spectra at multiple operating speeds. In some instances there is a close match between the predicted mode frequency and a peak in the vibration spectra. In these cases the motor is thought to be at or near a critical speed. At non-critical speeds the spectral peaks are seen to be near but not perfectly matching the predicted resonant frequencies. The agreement in the frequency of peaks in the acoustic spectra, surface displacement spectra, and simulated resonance frequencies indicates the model is capturing the rotor vibrations that are generating the acoustic tones. This will serve as a building block towards a model that can predict the resonant modes for UAM scale electric motors. This model would form the basis of a tool to predict electric motor noise in a system analysis type study.

Further exploration of rotor vibrations in different motors is planned. This future work will provide understanding of more complex mode shapes and also the applicability of the methods described here to other motor architectures.

Acknowledgments

This work was supported by NASA's Revolutionary Vertical Lift Technology (RVLT) project in the Advanced Air Vehicles Program.

References

[1] Rizzi, S.A., et al., "Urban Air Mobility Noise: Current Practice, Gaps, and Recommendations," NASA TP-2020-5007433, October 2020.

[2] Zawodny, Nikolas S., D. Douglas Boyd Jr, and Casey L. Burley. "Acoustic characterization and prediction of representative, small-scale rotary-wing unmanned aircraft system components." *72nd American Helicopter Society International Annual Forum*, West Palm Beach, FL, 2016, pp. 34-38.

[3] Intaratep, Nanyaporn, et al. "Experimental study of quadcopter acoustics and performance at static thrust conditions." *22nd AIAA/CEAS Aeroacoustics Conference*. 2016.
doi: 10.2514/6.2016-2873

[4] Gieras, Jacek F., Chong Wang, and Joseph Cho Lai. *Noise of polyphase electric motors*. CRC press, 2005.
doi: 10.1201/9781420027730

[5] Gieras, Jacek F., et al. "Analytical prediction of noise of magnetic origin produced by permanent magnet brushless motors." *2007 IEEE International Electric Machines & Drives Conference*. Vol. 1. IEEE, 2007.
doi: 10.1109/IEMDC.2007.383568

[6] Lopes, L.V., Burley, C.L., "ANOPP2 User's Manual," NASA/TM-2016-219342, October 2016.

[7] Bryan, George H. "On the beats in the vibrations of a revolving cylinder or bell." *Proceedings of the Cambridge Philosophical Society*. Vol. 7. No. 24. 1890.

[8] Huff, D. and Henderson, B. "Electric Motor Noise from Small Quadcopters: Part I – Acoustic Measurements," *28th AIAA/CEAS Aeroacoustics Conference*, 2018.
doi: 10.2514/6.2018-2952

[9] Henderson, B., Huff, D., Cluts, J., and Ruggeri, C. "Electric Motor Noise from Small Quadcopters: Part II – Source Characteristics," *28th AIAA/CEAS Aeroacoustics Conference*, 2018.
doi: 10.2514/6.2018-2953